



CORROSION OF COPPER-COATED STEEL HIGH LEVEL NUCLEAR WASTE CONTAINERS UNDER PERMANENT DISPOSAL CONDITIONS



Thalia Standish^a, Jian Chen^a, Rebecca Jacklin^b, Pellumb Jakupi^a, Sridhar Ramamurthy^{b,*}, Dmitriy Zagidulin^a, Peter Keech^c, David Shoemsmith^{a,b}

^a Department of Chemistry, Western University, London, Ontario, N6A 5B7, Canada

^b Surface Science Western, Western University, London, Ontario, N6G 0J3, Canada

^c Nuclear Waste Management Organization, Toronto, Ontario, M4T 2S3, Canada

ARTICLE INFO

Article history:

Received 14 April 2016

Received in revised form 17 May 2016

Accepted 19 May 2016

Available online 21 May 2016

Keywords:

Copper-coated steel

Nuclear waste container

Corrosion

Cold spray

Electrodeposited

ABSTRACT

The corrosion of high level nuclear waste containers under permanent disposal conditions can occur via a number of processes which change in importance as the environment within a deep geologic repository evolves from oxic to anoxic. The container design involves a copper coating on a steel vessel. The characteristics of these coatings are being assessed using standard analytical methods, including microscopy and electron backscatter diffraction. The corrosion processes on the surface of the coatings and at through-coating defects are also being investigated electrochemically. Although minor differences exist, the surface corrosion of cold sprayed and electrodeposited coatings generally exhibited similar corrosion behaviour to standard wrought copper. Corrosion at the base of a simulated through-coating defect in a cold-sprayed coating was found to proceed via galvanic coupling to oxygen reduction on the coating surface. Besides accumulating damage at the base of the defect, corrosion propagated along the copper/steel interface, most likely a consequence of the damage inflicted during the deposition process.

© 2016 The Authors. Published by Elsevier Ltd. This is an open access article under the CC BY license (<http://creativecommons.org/licenses/by/4.0/>).

1. INTRODUCTION

Like many nuclear nations, Canada has been investigating geological disposal of nuclear waste since the early 1970s, as this approach offers the best passive safety system for permanent disposal. The internationally accepted design of a deep geologic repository (DGR) involves disposal of the used fuel at a depth of ≥ 500 m in a suitably dense intact rock. To ensure containment, the nuclear fuel will be sealed in a corrosion resistant used fuel container (UFC) capable of withstanding the anticipated hydrostatic, lithostatic and glaciation loads. To provide an additional barrier, the UFC will be surrounded by compacted bentonite clay which swells on contact with moisture to tightly seal the system and provide a local environment in which only very little chemical diffusion can occur. A schematic representation of the proposed Canadian DGR is shown in Fig. 1.

The original Canadian UFC was very similar to the Scandinavian KBS-3 container and designed to contain 260 CANDU fuel bundles, which are ~ 50 cm in length and 10 cm in diameter (Fig. 1). These dual-walled containers are designed with an inner iron (or steel)

bolted vessel to provide strength, and a separately fabricated 25–50 mm-thick Cu outer shell corrosion barrier. The dimensions of this shell are dictated by the container fuel capacity and manufacturing requirements, a significant wall thickness being necessary to provide sufficient stiffness to avoid warping of a shell this size. However, conservative estimates [1] suggest only a small fraction of this available thickness will be required as a corrosion allowance (≤ 1.3 mm over 10^6 years) even in groundwater containing unexpectedly high concentrations of sulphide (i.e., 3 ppm), which is known to corrode Cu.

Beginning in 2011, the Nuclear Waste Management Organization (NWMO) initiated a program to incorporate Scandinavian efforts to improve container design and to take advantage of recent improvements in manufacturing technologies and the unique small size of the CANDU fuel bundle. Presently, two conceptual designs are under consideration, Fig. 2. The 288 CANDU bundle Mark 1 retains the original Canadian design but has been altered to more closely align with the Scandinavian design with respect to geometry, enabling the transfer of technology between the two programs. However, manufacturing challenges remain with this design. To overcome these issues, while taking advantage of the CANDU bundle dimensions, the 48 bundle Mark 2 design, which utilizes an integral Cu coating on a fully welded steel container, is

* Corresponding author. Tel.: +5196612173; fax.: +5196613709.

E-mail address: sramamur@uwo.ca (S. Ramamurthy).

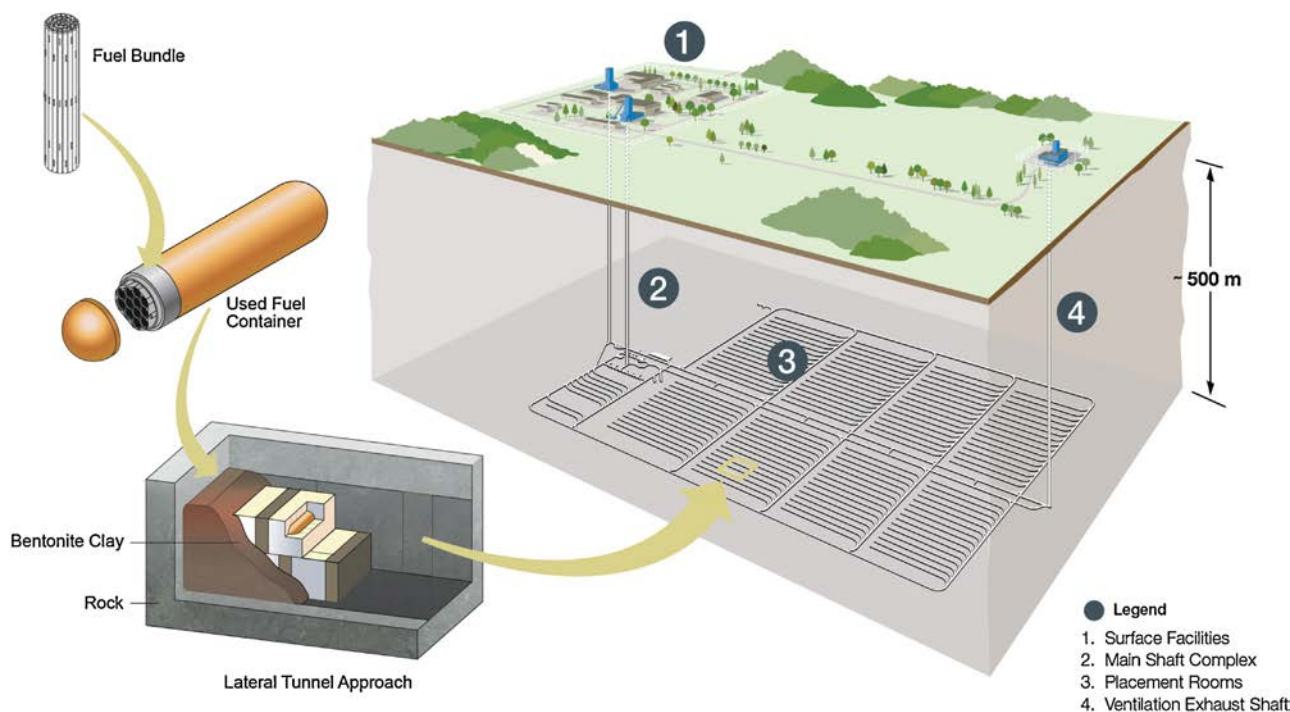


Fig. 1. Schematic representation of the proposed Canadian Deep Geologic Repository (DGR).

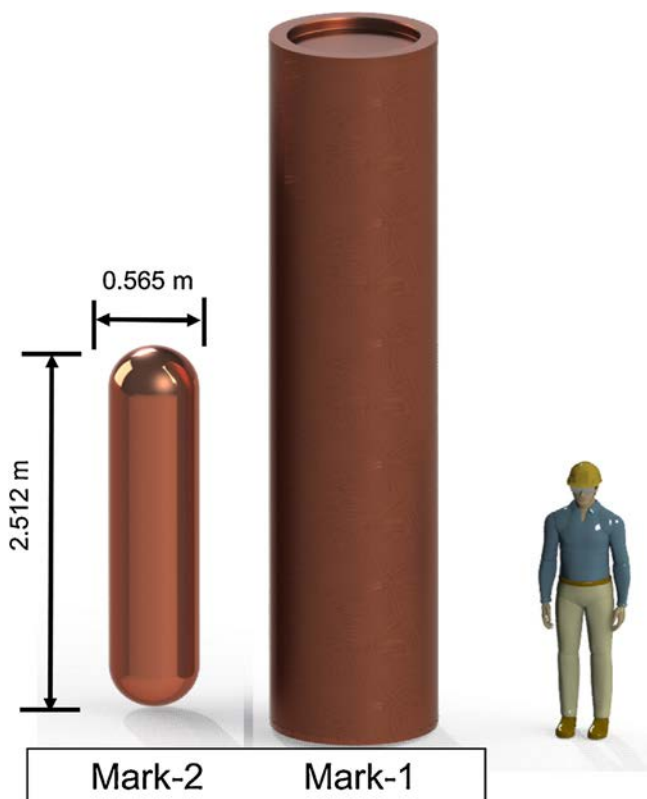


Fig. 2. The two conceptual container designs under consideration for the disposal of Canadian high level nuclear waste.

being considered. As depicted in Fig. 2, the Mark 2 is also substantially shorter (and lighter) than the Mark 1 which offers flexibility in handling. The use of commercial processes such as

cold spray coating and electrodeposition are being considered [2,3] and since the required corrosion allowance is small, the corrosion performance of coatings with a thickness of a few mm is being evaluated [4].

Any chosen repository location must obviously be geologically stable and possess clearly identifiable advantageous features, which must not be permanently damaged by the thermal/chemical transient imposed by the excavation and waste emplacement process. Additionally, the evolution of the repository from the initially disturbed to the final long term condition must be predictable with reasonable certainty. While total corrosion is expected to be very small in a repository, the conditions within a Canadian repository will evolve from an initially aggressive initial state to an eventually benign state, Fig. 3. Upon repository closure, the temperature of the container surface will rise due to the heat produced by the radioactive decay of the spent fuel waste form in the container. It will also be oxidizing due to a combination of a small amount of oxygen, introduced during the period of repository excavation and emplacement of the waste, and the potential production of radiolytic oxidants due to gamma radiolysis of the environment. However, the rise in temperature will produce a low humidity environment in the vicinity of the container and negligible corrosion would be expected despite the oxidizing conditions.

Subsequently, moisture will return as the containers cool until full resaturation of the local environment is achieved. The period required for resaturation (i.e., the establishment of a relative humidity (RH) = 100%) is uncertain but expected to be between 20 and 100 years for a crystalline repository (as indicated in Fig. 3) but much longer for a sedimentary clay repository (i.e., >1000 years). Also, it is possible resaturation will occur non-homogeneously and rewetting of the surface will not be uniform. As resaturation progresses, trapped O₂ will be consumed by Cu corrosion, reactions with minerals and organic material in the clay, and biological processes. Consequently, repository conditions will evolve from

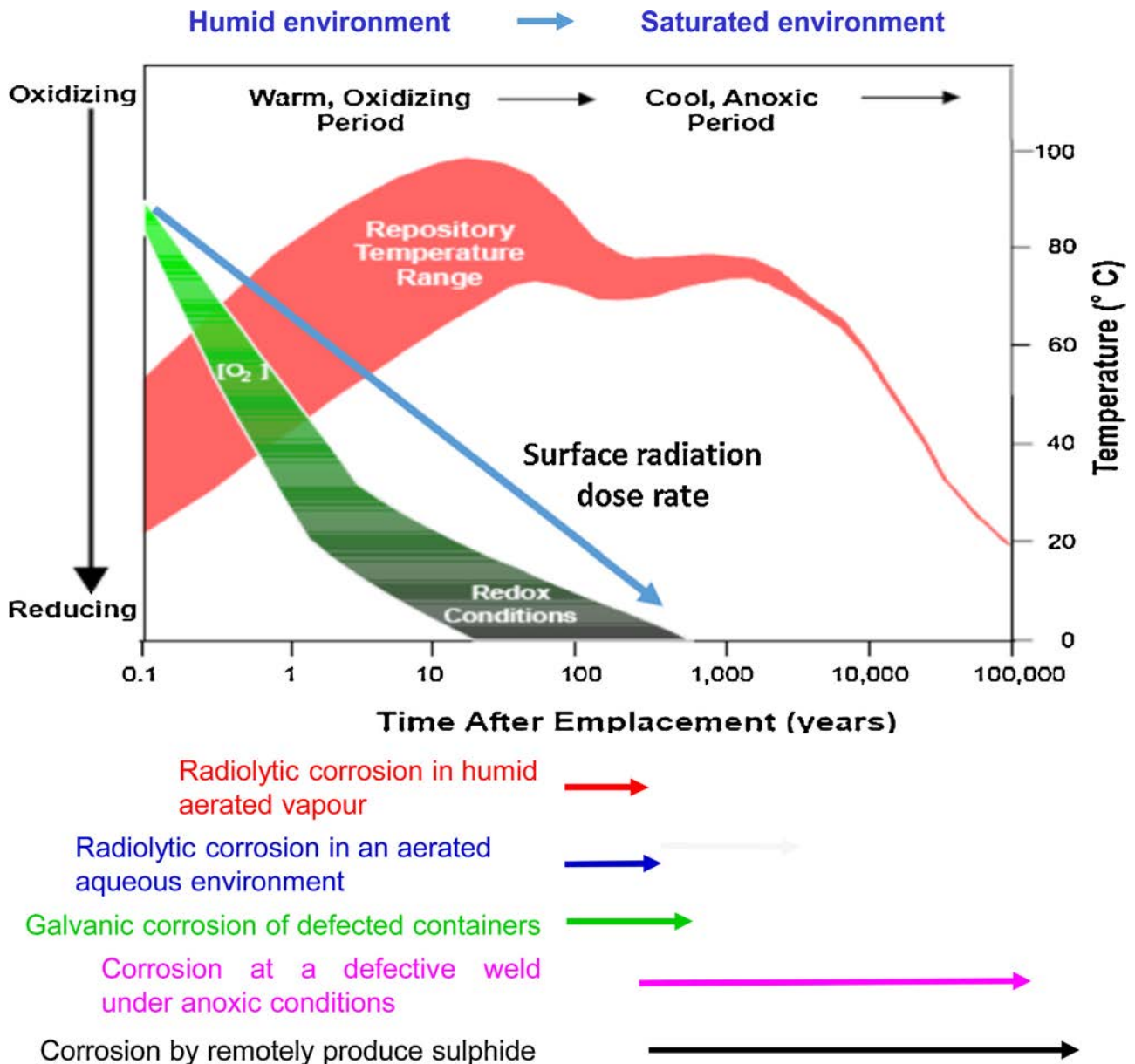


Fig. 3. Schematic illustration showing the evolution of exposure conditions anticipated in a Canadian DGR. Also shown are the approximate time periods for the various possible corrosion processes.

warm and oxidizing to cool and anoxic over an uncertain period of a few months to many hundreds of years.

- As resaturation occurs the prospects for corrosion increase and four different, but not necessarily well-defined, container exposure periods can be defined: (i) aerated vapour but no condensed H_2O on the Cu surface; (ii) aerated vapour in equilibrium with a condensed H_2O -based solution layer on the surface; (iii) anoxic or close to anoxic, conditions with either H_2O vapour in equilibrium with a condensed H_2O layer or a fully resaturated condition; and (iv) a fully anoxic H_2O -saturated condition. The duration of each period may be different for different areas of the container surface, although, given the pathways by which O_2 can be consumed, the redox conditions in the critical periods (ii) and (iii) are difficult to specify.

As indicated in Fig. 3, the evolution of Cu surface redox conditions will be influenced by the gamma (γ) radiation emitted by the fuel wastefrom inside the container. Since the γ -dose rate is

dominated by the decay of the fission products in the fuel, and is calculated to vary from ~ 5 Gy/h after 10 years to ~ 0.44 Gy/h after 200 years. Consequently, γ -radiation could influence surface redox conditions, and hence corrosion processes, to a greater and eventually lesser degree over periods (i) through (iii).

Based on this evolution of repository conditions, the possible corrosion processes can be defined as shown schematically in Fig. 4, with the expected time periods over which they would be expected illustrated in Fig. 3. Notably, during the critical resaturation period γ -radiation fields could remain significant leading to radiolytically-assisted corrosion processes under both aerated humid vapour and resaturated aqueous conditions.

Once anoxic conditions have been established (i.e., available O_2 has been consumed and γ -radiation fields are insignificant), the only remaining source of oxidant would be dissolved sulphide produced by microbial processes, in particular, the action of sulphate reducing bacteria, or by dissolution of sulphide minerals

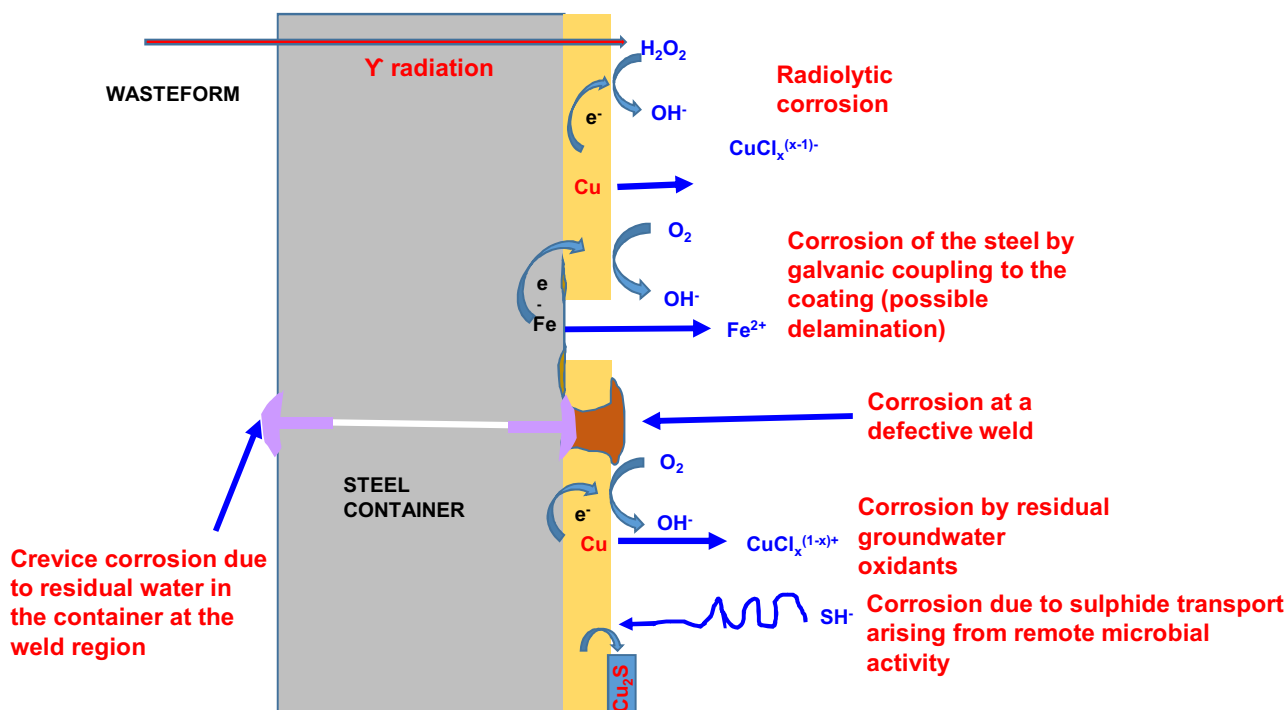


Fig. 4. Possible corrosion processes on a high level nuclear waste container in a deep geologic repository.

within the clay. The production of sulphide is likely to occur at locations remote from the container surface since the population of the Cu surface by biofilms will be prevented by the immobility of microbes within the narrow pores in the highly compacted bentonite clay and the low water activity in the vicinity of the container surface. Since the corrosion of Cu in aqueous sulfide solutions has been shown to be rapid [5–7], it is likely this corrosion process will proceed under sulphide diffusion control.

One additional corrosion process could bypass the Cu coating if the container is emplaced in the repository with a through-coating defect, a situation which should be avoided by proper inspection of the container prior to emplacement. Although illustrated separately in Fig. 4, the most problematic location for such a defect is in the area of the closure weld in the steel, since the total container wall thickness at this location will only be 8 mm compared to that on the container wall (47 mm) and the hemispherical head (30 mm). Immediate exposure of the steel substrate during the early oxidizing period of the repository would lead to galvanic corrosion with steel dissolution at the base of the defect being driven by O_2 reduction on the adjacent Cu surface. Such a process is unlikely to continue for an extended period of time since the supply of dissolved O_2 will be consumed fairly quickly in the region near the coating defect.

Finally, if water is trapped within the container on sealing, some corrosion damage would accumulate on the container's internal steel components. Since the maximum volume of trapped water would be small, even for scenarios that assume many damaged fuel bundles, most corrosion mechanisms (i.e. general corrosion) cannot be significantly damaging to the container. Accordingly, problematic corrosion is restricted to within the occluded region near the weld, where the container lid and body are joined, as the accumulation of corrosion product could, in principle, produce stress upon the weld. While such damage could be eliminated by removal of H_2O from the container prior to sealing, pessimistic assumptions regarding fuel cladding integrity necessitate welds

that can tolerate these processes, especially where radiation is present. Recent studies indicate this process is unlikely to lead to significant damage accumulation [8].

In this publication, the properties and corrosion performance of Cu coatings formed either by cold spray deposition or electrodeposition are reported under anoxic and aerated-to-anoxic conditions. The corrosion performance of the coated steel containing a through-coating defect allowing the establishment of a galvanic couple is also investigated. This last study can be considered the first step in developing a model for the failure of a defective container. The influence of sulphide on the long term durability of the container is also under study but is not discussed in this publication.

2. EXPERIMENTAL METHODOLOGY

Coated steel specimens were supplied by the Surface Technologies Group (Advanced Forming and Coatings Division) of the National Research Councils' Industrial Materials Institute (Boucherville, Québec), and a detailed description of the process may be found elsewhere [9]. Samples were deposited on 25 mm thick, A516 Grade 70 steel grit blasted with 24 grit alumina, with PCS-800 or PCS-1000 (Plasma Giken Co., Ltd., Toshima-ku, Tokyo) systems, using He and N_2 as the accelerating gases for bond coat and subsequent coats, respectively. As noted by Vo et al., the bond coat was required to obtain adhesion between the Cu and steel materials. Two differently prepared cold sprayed Cu samples were examined: (i) one with a 3 mm coating used as prepared; (ii) a coating with the same thickness which was subsequently annealed at 350°C for 1 hour under an Ar atmosphere. Electrodeposited samples were provided by Integran Technologies Inc. (Mississauga, Ontario), also with a 3 mm thick coating [10]. Wrought Cu specimens (P-doped and O-free) were supplied by the Swedish Nuclear Fuel and Waste Management Company (SKB, Stockholm, Sweden).

Specimens used in corrosion experiments were polished on all sides using SiC paper (using water), and a 3 micron diamond paste suspension (using varsol). For the samples monitored electrochemically, a stainless steel wire was soldered to the back of the sample and heat shrink tubing was applied onto the wire with a heat gun. The sides and backs of the samples were subsequently painted with three coats using an Amercoat™ epoxy resin, allowing each of the coats to cure in an oven at 60 °C for 24 hours, such that one copper face was exposed. Following curing, the exposed face was again polished using a 3 micron diamond paste suspension. The electrodes designed to investigate a simulated coating defect were prepared by drilling a 500 μm diameter hole through a cold spray coated specimen to expose the Cu/steel interface, Fig. 5(a). The top surface of the Cu was wet polished to a 1200 grit finish with SiC paper while making sure no H₂O came into contact with the steel substrate at the base of the hole. A stainless steel current collecting wire was spot welded to the steel substrate after which heat-shrink Teflon tubing was used to cover the wire. The electrode was then sonicated in methanol and painted with Amercoat leaving only the top Cu surface with the drilled hole exposed, Fig. 5(b). The Cu surface was then wet polished with SiC to a 2400 finish, rinsed with methanol and dried in a stream of N₂ prior to an experiment.

Electrochemical measurements were performed in a standard three electrode cell with a saturated calomel reference electrode (SCE) and a Pt foil counter electrode on annealed cold spray (CSA), electrodeposited (ED) and SKB wrought Cu (SKB) electrodes. Additional specimens were placed in the cell and removed at different times for analyses. Corrosion potential (E_{CORR}) and linear polarization resistance (R_p) measurements were performed at 10 mV/min using Solartron potentiostats and Corrview™/Corrview™ software. Experiments were conducted in a 3 M NaCl solution purged with either high purity O₂ or Ar, or in an anaerobic chamber. Long-term electrochemical experiments were performed on CSA, ED and SKB samples exposed to a 3 M NaCl solution for a period of 150 days or greater. Additional samples were placed in the cell and removed periodically for analysis.

Scanning electron microscopy (SEM) and energy dispersive X-ray spectroscopy (EDX) were performed using a Hitachi S-4500 field emission SEM equipped with a Quartz XOne EDX system. Raman spectroscopy was performed using a HeNe laser with a wavelength of 632.8 nm which produces a focussed beam ~2 μm in diameter at the sample surface.

3. RESULTS AND DISCUSSION

3.1. Characterization of Coatings

Figs. 6(a) and 6(b) show the surface of the CSA coating before and after polishing. The form of the originally deposited particles (~20 μm to ~60 μm in size) is clearly visible on the surface and is not completely removed by the polishing. Fig. 6 (c) shows an SEM micrograph of a polished cross section illustrating the deformation of the Cu/steel interface incurred during particle impact. Figs. 7 (a) and (b) show the unpolished surface of the ED coating and a polished cross section of the Cu/steel interface. The surface contains a significant submicron porosity, but examination of cross sections shows this is limited to the top ~25 μm and does not permeate the full coating thickness. The polished cross section shows the Cu/steel interface is uniform and undamaged.

Fig. 8 shows electron back scatter diffraction (EBSD) images for a cold spray Cu coating, annealed at 450 °C for 4 hours, and an electrodeposited coating. Prior to annealing, the cold spray coated specimen exhibited an extremely small grain size and the particle impact pattern was clearly visible in the images [3]. Post annealing, the grain size was increased by a factor of 4 and a significant number of Σ3 coincident site lattice boundaries were formed. Additionally, the irregularity of the steel/coating interface is clear and the black locations within the coating indicate the presence of voids formed by the coalescence of microporosity during annealing. The EBSD map for the electrodeposited specimen shows the average grain size is approximately twice that of the annealed cold spray specimen, and texture is present along the low energy <111> planes. A majority of the grain boundaries exhibit Σ3 coincident site lattices and a thin layer of smaller crystals is present at the steel interface. The misorientation maps, Fig. 9, show that significant plastic strain is present in the original cold spray coating, prior to annealing, and that the coating/steel interface is heavily damaged by particle bombardment. Annealing leads to a considerable reduction in strain and a more regular coating/substrate boundary. The electrodeposited coating is relatively strain-free except for the thin layer comprised of small grains located at the Cu/steel interface. Although not shown here, the wrought Cu (SKB) specimens exhibited large grain sizes (~100 μm) with some twinning.

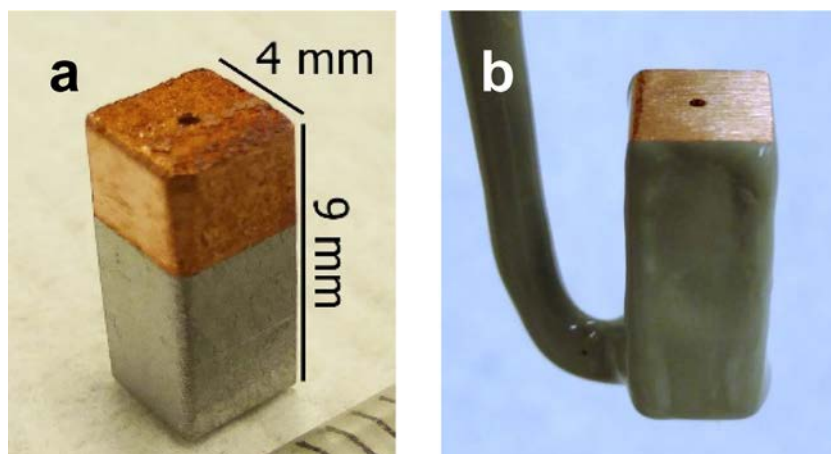


Fig. 5. Cu-coated steel sample with a hole drilled through the copper to the steel, a) uncoated, b) with a wire connector and coated with Amercoat.

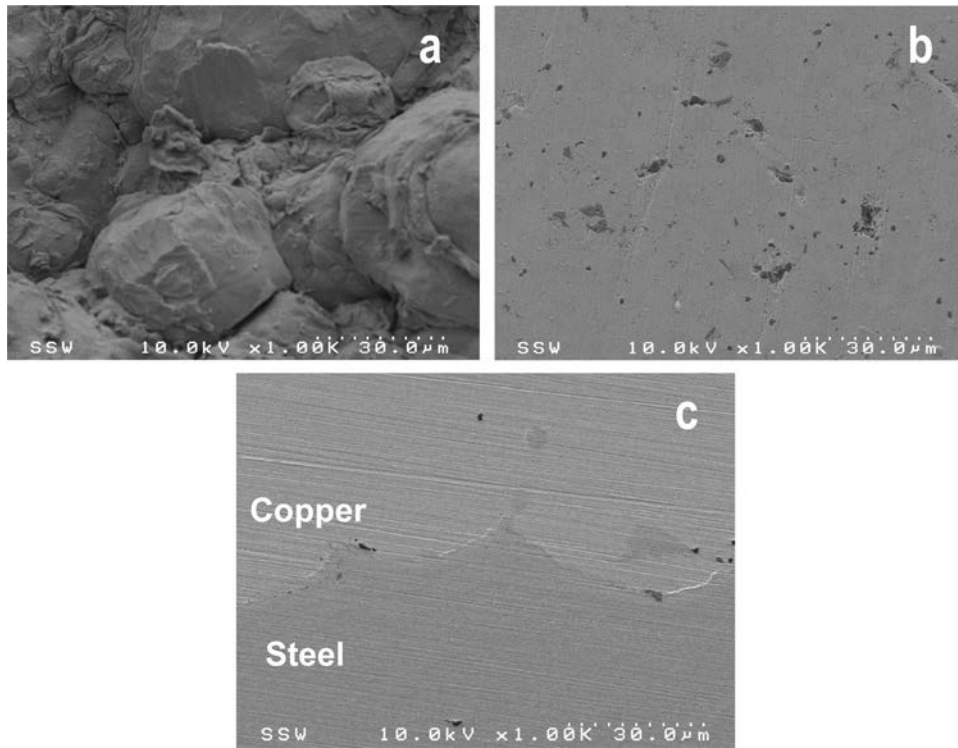


Fig. 6. SEM micrographs of a CSA specimen: (a) unpolished surface; (b) polished surface; (c) polished cross section showing the Cu/steel interface.

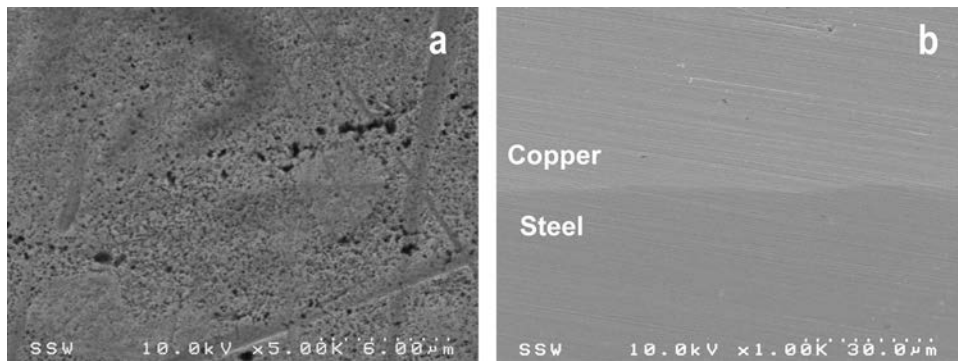


Fig. 7. SEM micrographs of an ED specimen; (a) the unpolished surface; (b) a polished cross section of the Cu/steel interface.

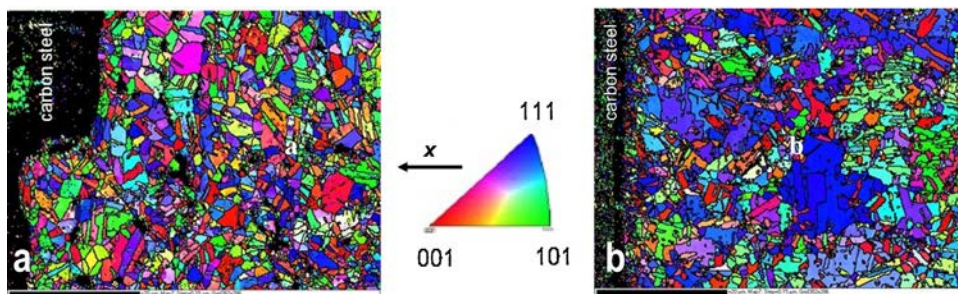


Fig. 8. EBSD images recorded on cross sections of an: (a) CSA; and (b) ED coating.

3.2. Corrosion of the Coatings

Fig. 10 shows corrosion potential (E_{CORR}) and polarization resistance (R_p) values measured on the CSA, ED and SKB specimens

with the electrochemical cell placed inside an anaerobic chamber. The concentration of dissolved O_2 was estimated to be ≤ 0.042 ppb [4]. The E_{CORR} values for all three specimens are very similar and effectively constant within the range from -370 to -375 mV,

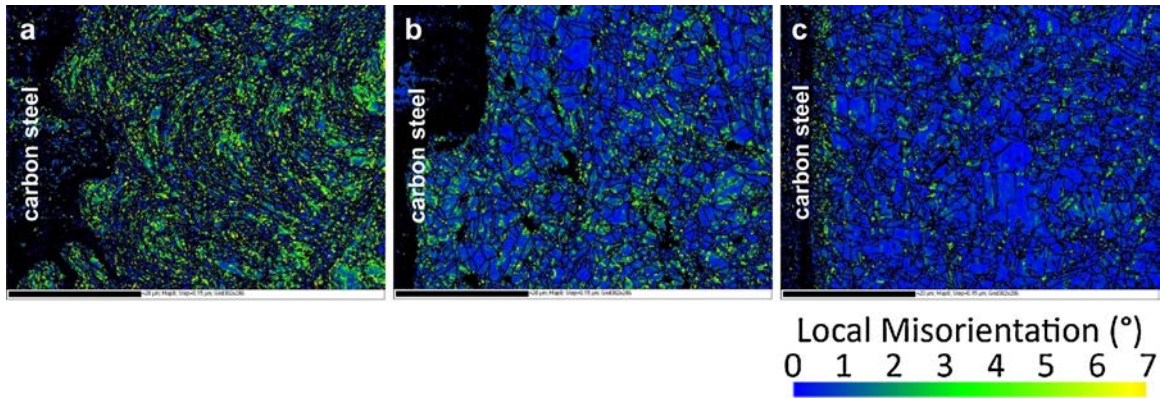


Fig. 9. Misorientation (plastic strain) maps recorded on cross sections of an (a) unannealed cold spray coating; (b) a CSA coating; and (c) an ED coating.

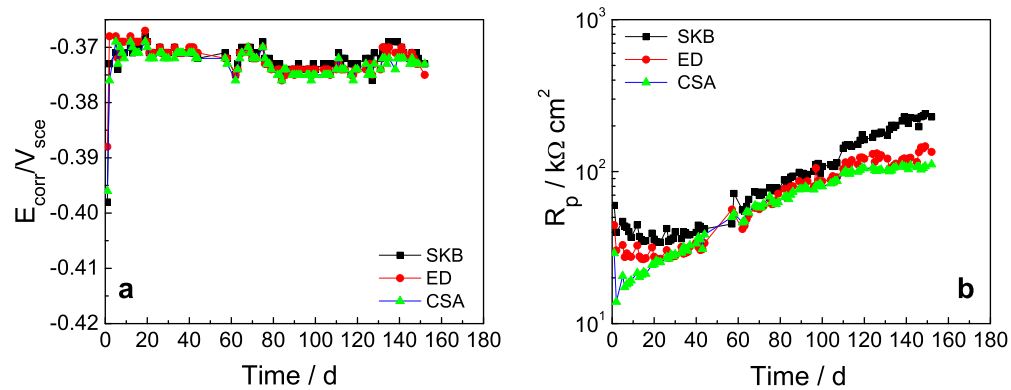


Fig. 10. Evolution of (a) corrosion potential (E_{CORR}) and (b) polarization resistance (R_p) with time for CSA, ED and SKB electrodes measured in a 3 M NaCl solution in an anaerobic chamber.

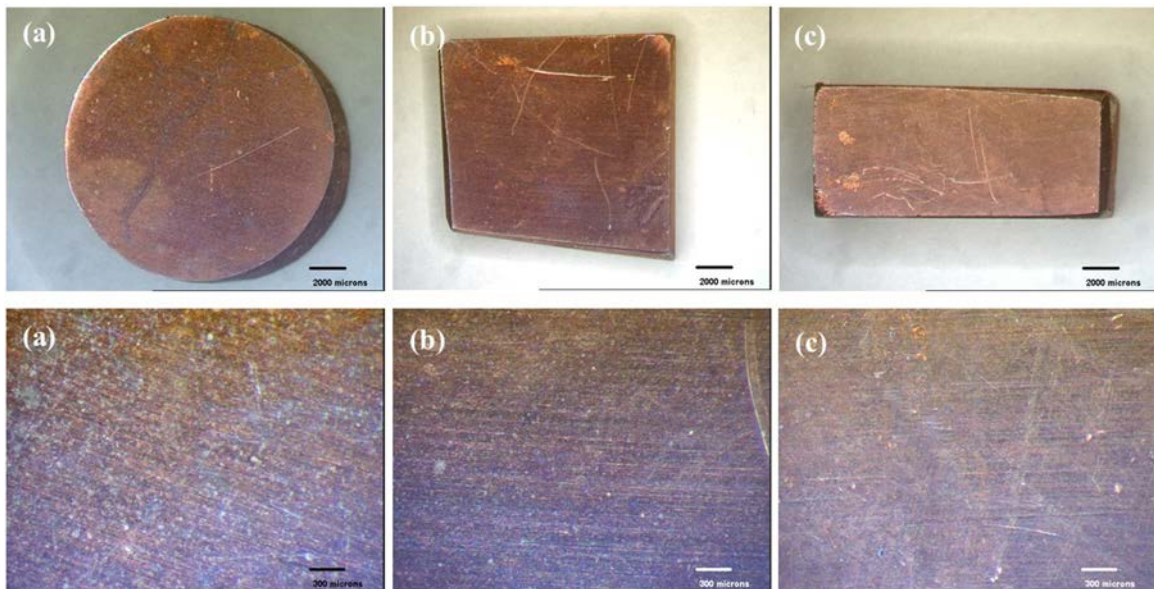


Fig. 11. Optical micrographs recorded on the (a) CSA; (b) ED; and (c) SKB after exposure to a 3 M NaCl solution in an anaerobic chamber.

consistent with the maintenance of anaerobic conditions [11,12]. The similarity in values indicates that, despite the differences in surface conditions, all three electrodes behave effectively the same.

The R_p values are initially low (20 to 40 $\text{k}\Omega \cdot \text{cm}^2$) but increase steadily to $\geq 100 \text{k}\Omega \cdot \text{cm}^2$ over the 160 day exposure period, with the value for the SKB electrode becoming approximately a factor of 2 greater than for the other two electrodes. At short exposure

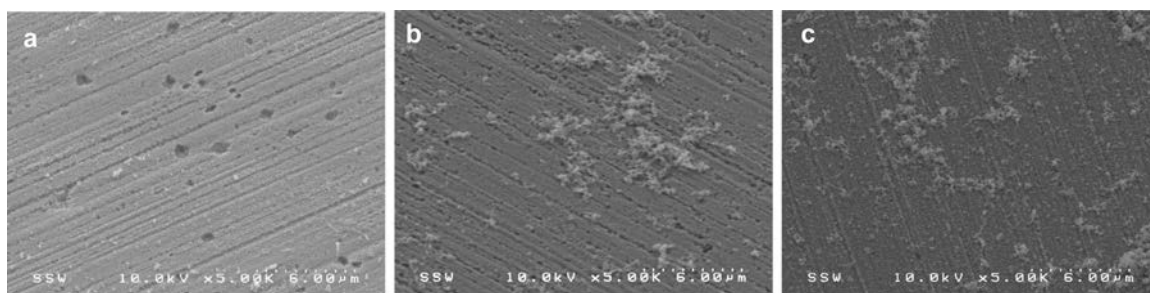
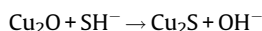


Fig. 12. SEM images of the CSA; (b) ED and (c) SKB electrodes after exposure to a 3 M NaCl solution in an anaerobic chamber.

times, the R_p values differ markedly. Since all three electrodes are polished to the same finish, these differences are not attributable to significant differences in the surface areas of the specimens (the measured values were normalized to the geometric areas).

Optical micrographs of the specimen surfaces, Fig. 11, show no visible signs of corrosion, although SEM images, Fig. 12, show the accumulation of a fine, widely distributed deposit. The fine network of minor pits on the ED specimen and the wider distribution of minor pits on the CSA specimen are not corrosion signatures but reflect the state of the surface prior to exposure to the solution. Energy dispersive X-ray analyses (EDX) and X-ray photoelectron spectroscopy (XPS) show the presence of S and Raman spectroscopy confirms the presence of Cu_2S (chalcocite) (a peak at 284 cm^{-1}), the expected product when Cu is corroded in sulphide-containing solutions [6,13]. The origin of the sulphide is most likely as an impurity in the NaCl used to prepare the solutions, since sulphide is used to remove trace heavy metals from NaCl during the production of high purity NaCl. Since the $[\text{Cl}^-]$ is so high in the solutions used in corrosion experiments (i.e. 3 M), significant total quantities of sulphide may be present in the solution volume, and would react rapidly with the Cu surface, accumulating as chalcocite.

The observation of this trace sulphide on the copper surfaces then offers a possible explanation for the initially low but eventually increasing R_p values, Fig. 10. The specimens are undoubtedly covered with a surface oxide ($\text{Cu}_2\text{O}/\text{CuO}$) on first exposure to the 3 M NaCl. This oxide has been shown to be unstable in the presence of dissolved SH^- and would convert to Cu_2S most likely via a direct chemical process [13],



Subsequent reactivity may be derived from the reaction of SH^- with the exposed Cu surface,



This latter reaction has been shown to be rapid [14] and would proceed under diffusion control in the presence of trace concentrations of SH^- . This sequence of reactions could account for the initial decreases in R_p and the subsequent slow increases as the SH^- impurity in the solution was depleted.

To simulate the evolution of repository conditions from initially aerobic to eventually anoxic (Fig. 3), another set of Cu specimens were exposed to O_2 -purged conditions for 61 days and then to Ar-purged conditions for a further 117 days. The E_{CORR} and R_p values are shown in Fig. 13 for all three specimens. As expected, the E_{CORR} values increased during the aerobic period from $\sim -320\text{ mV}$ to ~ -200 to $\sim -250\text{ mV}$. This coincided with the accumulation of corrosion product deposits as observed visually. The E_{CORR} values for all three specimens were erratic, a feature attributed to periodic delamination of patches of corrosion product from the electrodes which were suspended with the exposed surface face downwards. Delamination was observed for all three electrodes but was particularly pronounced on the ED and SKB specimens. The time period of the fluctuations suggests delamination is a slow process probably involving the slow undermining of the deposit by the penetration of electrolyte.

Fig. 13(b) shows the R_p values initially increase rapidly, periodically achieving values as high as $200\text{ k}\Omega\cdot\text{cm}^2$. The periodic increases and decreases in R_p values coincide with the fluctuations in E_{CORR} as indicated for the ED specimen in the inset in Fig. 13(a), with high R_p values coinciding with low E_{CORR} values. These variations are consistent with the formation and periodic delamination of the corrosion product deposits, the high values

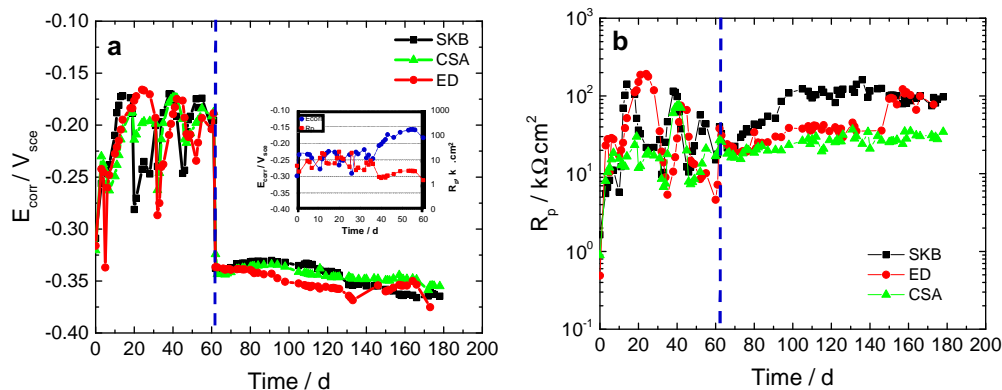


Fig. 13. Evolution of (a) E_{CORR} and (b) R_p with time on CSA, ED, and SKB electrodes exposed to an O_2 -purged 3 M NaCl solution up to 61 days and then to the same solution but Ar-purged.

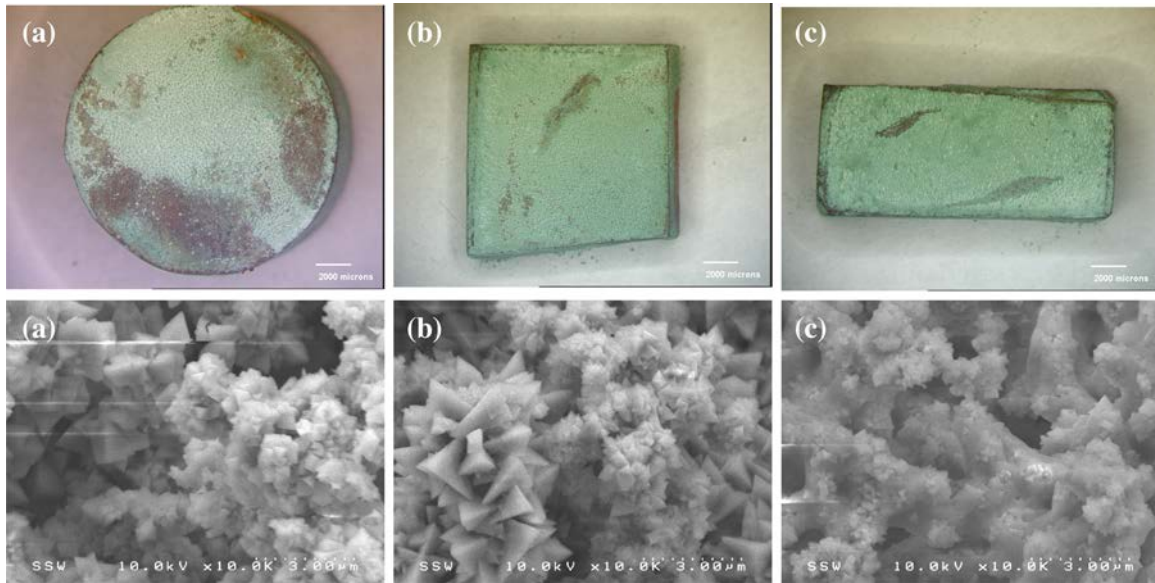


Fig. 14. Optical and SEM images of (a) CSA; (b) ED and (c) SKB electrodes exposed to an O₂-purged 3 M NaCl solution for 61 days.

being achieved when a coherent deposit is present and the corrosion rate is low, and low values after delamination when the corrosion rate increases. The patchy nature of the green deposit is consistent with the occurrence of delamination.

Fig. 14 shows the surfaces of the three specimens extracted from this experiment after the oxygenated period of 61 days. Since these specimens were face-up in the electrochemical cell, they are more uniformly covered with a green deposit shown (by X-ray diffractometry) to be atacamite (Cu₂(OH)₃Cl), as expected for Cu corrosion in aerated/oxygenated chloride solutions [15–18]. Under these conditions the general corrosion reaction is well-known, and can be written

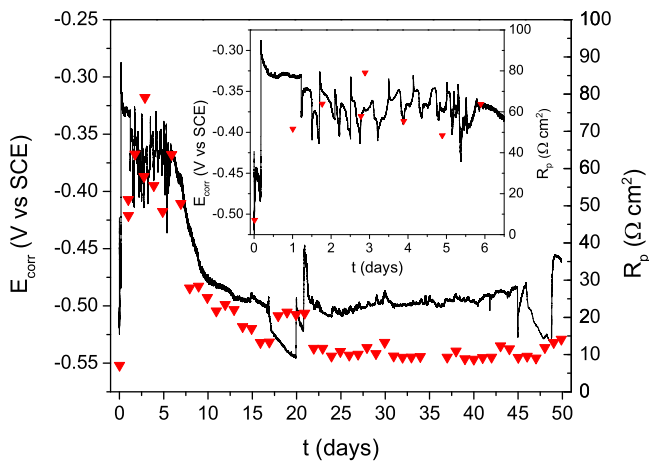
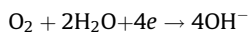
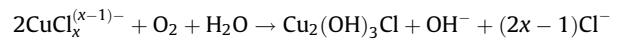


Fig. 15. E_{CORR} (black line) and R_p (red triangles) data for an unannealed cold sprayed electrode with a through coating defect (Fig. 3) exposed to an O₂-purged 3 M NaCl solution. The inset shows an expanded view of the E_{CORR} and R_p data recorded over the first 6.5 days.

Subsequently, homogeneous oxidation to produce Cu²⁺ occurs [18] leading to the deposition of Cu(II) solids, in particular atacamite,



On switching to anoxic conditions (for times >the vertical dashed line in Fig. 13), E_{CORR} for all three specimens decreased to ~-340 mV and then, over the subsequent exposure period, slowly to ~-360 mV to -375 mV; i.e., to E_{CORR} values close to those observed in the totally anoxic experiment (Fig. 10). This slow decrease is accompanied by an increase in R_p values, Fig. 13, especially for the SKB specimen. Except for the ED specimen, the R_p values approach the values measured under totally anoxic conditions (Fig. 10(b)). The increase in R_p values over the 30 day period immediately following the switch to Ar-purged conditions could be a consequence of the local reduction of surface Cu^{II} species by reaction with the Cu substrate as proposed by King et al. [12]. In the concentrated Cl⁻ solution, this reaction would lead to the formation of soluble CuCl_x^{(x-1)-} species and further exposure of the Cu substrate as conditions more closely approached those under anoxic conditions.

3.3. Corrosion of Defective Coatings

Fig. 15 shows the E_{CORR} and R_p values recorded in an aerated 3 M NaCl solution using the electrode containing a simulated defect (Fig. 5). Initially, E_{CORR} is in the range -420 mV to -520 mV and R_p is < 10 Ω·cm² indicating active corrosion of the steel. However, after ~4 hours, E_{CORR} increases (over a ~20 min period), accompanied by an increase in R_p, indicating a decrease in corrosion rate due to the deposition of a corrosion product film. Beyond a short stable period, both E_{CORR} and R_p become erratic with coincidental decreases (indicating film breakdown and acceleration of corrosion) and increases (indicating film deposition and suppression of corrosion). Eventually, E_{CORR} decreases over a 10 day period (5 to 15 days into the experiment) with an accompanying decrease in R_p, evidence for an irreversible loss of even minimal corrosion protection by a deposit. The temporary decreases in E_{CORR} (17 and 46 days) and subsequent increases are presumed to be due to temporary interruptions in O₂ bubbling and confirm that the steel

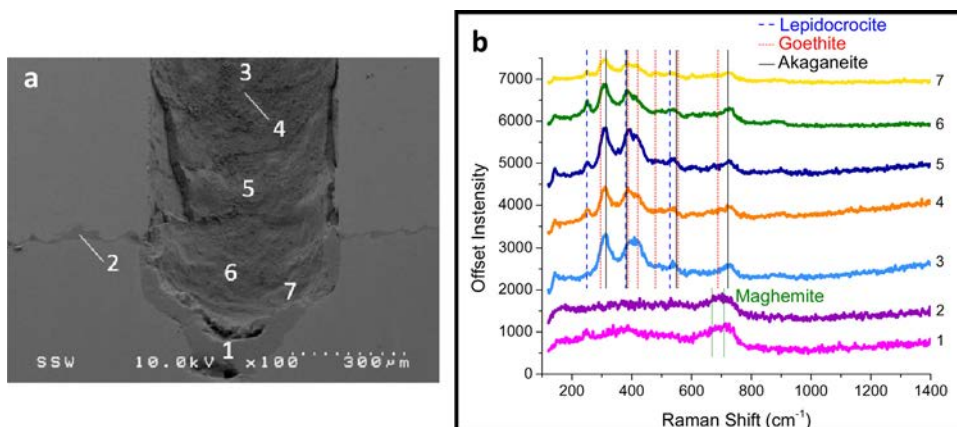


Fig. 16. (a) SEM image showing the base of the defect corroded in an O₂-purged 3 M NaCl solution for 24 hours; (b) Raman spectra recorded at the numbered locations in (a).

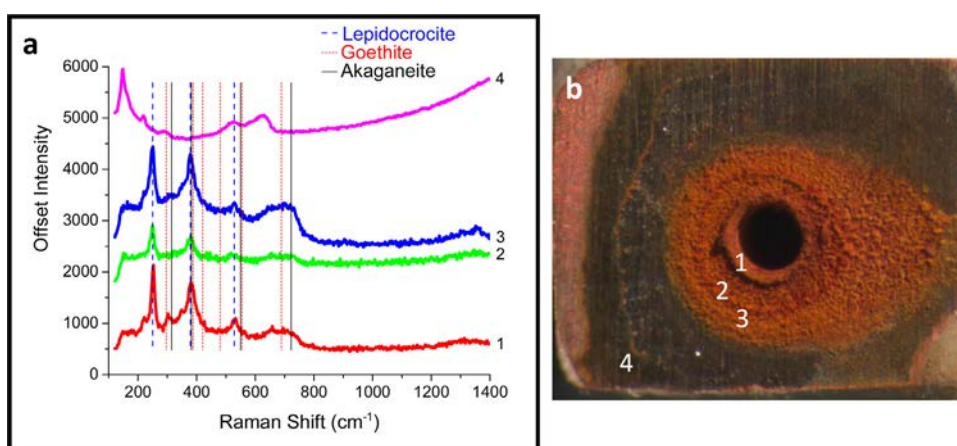


Fig. 17. Raman spectra (a) recorded at the numbered locations shown (b) on the Cu surface peripheral to the defect in the Cu coating.

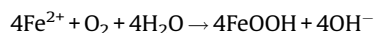
corrosion process is coupled to the supply of O₂ to the coupled Cu surface. In these intervals, a decrease in E_{CORR} is accompanied by an increase in R_p, consistent with cathodic control of the corrosion process.

To determine the composition of the corrosion products formed inside the coating defect, a specimen corroded for 24 hours in oxygenated 3 M NaCl was mounted in resin and cross-sectioned. Fig. 16 shows an SEM micrograph of the base of the defect (which penetrated slightly into the steel when first drilled) and a series of Raman spectra recorded at the numbered locations on the image. The image shows a substantial oxide film on the exposed steel surface (location 1). The two broad Raman peaks at 350 and 500 cm⁻¹ and the higher intensity peaks at 670 and 720 cm⁻¹ suggest the presence of maghemite, γ-Fe₂O₃ [19,20], as indicated by the vertical lines. However, the dominant A_{1g} mode of magnetite, Fe₃O₄ (670 cm⁻¹) [21] and a peak attributable to akaganeite (β-FeOOH) (723 cm⁻¹) [22] also occur in this region, making an unambiguous identification of the film impossible.

Raman spectra recorded at locations 3 to 6 all exhibit the same peaks but with some variation in the intensities of individual bands. The vertical coloured lines indicate the characteristic Raman shifts for lepidocrocite (γ-FeOOH) [19,23], goethite (α-FeOOH) [19,23], and akaganeite [20,22]. These phases are expected to form in the presence of O₂ and Cl⁻ and which phase is dominant depends on their solution concentrations and that of Fe²⁺ [22]. Environments with high [Cl⁻] (≥2 M) and high [Fe²⁺] (≥0.5 M) favour the formation of akaganeite, while lower [Fe²⁺]

favours lepidocrocite, and goethite forms when either [Cl⁻] or [Fe²⁺] is high while the other is low [22]. In solutions containing a high [O₂], lepidocrocite forms preferentially to goethite [22,24] but can transform to goethite with time [25]. Inside the defect, the corrosion product is a mix of the above 3 phases with the peaks for akaganeite being relatively the most intense. This would be expected for the high [Fe²⁺] and [Cl⁻] conditions likely to prevail within the defect. Figs. 15–17 indicate an evolution of redox conditions within the defect with immersion time. The universal formation of Fe^{III} oxyhydroxides at the base of the defect, on the walls of the coating, and on the external surface of the coating, indicates oxidizing conditions existed at short exposure times.

However, as shown in Fig. 17, a substantial amount of iron is transported out of the defect and deposited on the external Cu surface. For this to occur, transport would be as Fe²⁺ which has a solubility six orders of magnitude greater than Fe³⁺ in the near neutral pH range of these experiments. For this to occur, O₂ must become significantly depleted within the defect. As expected, Raman analyses show γ-FeOOH to be the dominant phase; once Fe²⁺ diffusing out of the defect encounters the high O₂ concentration prevailing in the bulk of the solution, with Fe^{III} oxyhydroxide deposits being formed by the homogeneous oxidation of Fe²⁺ to the much less soluble Fe³⁺ [26],



A Raman spectrum recorded on the Cu surface beyond the deposit (location 4, Fig. 17) shows the surface to be covered by

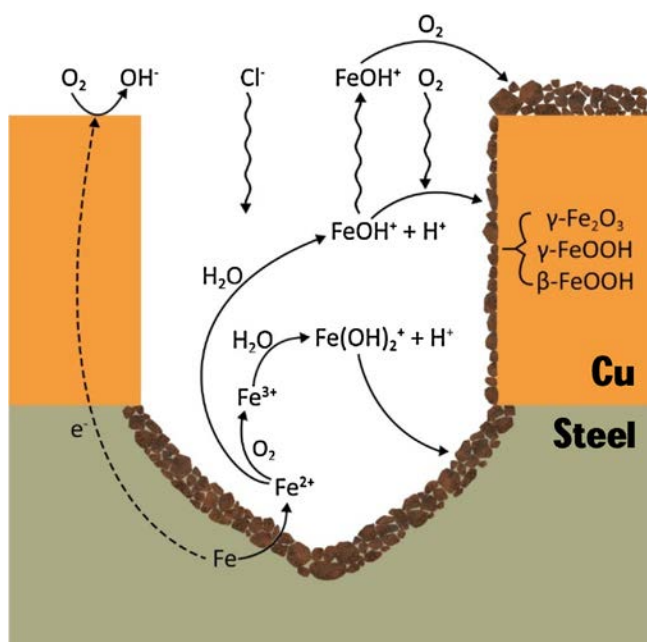


Fig. 18. Schematic illustration of the chemistry inside a coating defect during corrosion in an O_2 -purged 3 M NaCl solution.

Cu_2O , as indicated by the broad peak doublet between 490 and 650 cm^{-1} [27,28]. Since deposition of the Fe^{III} oxyhydroxides occurs outside the defect, O_2 must be depleted within it, avoiding extensive oxidation and deposition and allowing diffusive transport of soluble Fe^{2+} , thereby maintaining the active corrosion of the steel detected electrochemically. Transport of Fe^{2+} will also be facilitated by its hydrolysis within the defect at this Cl^- concentration by the presence of $FeCl^+$, although this is not shown in the schematic. Fig. 18 illustrates the conditions, equivalent to those in an active pit, prevailing within the defect.

The EDX map, Fig. 19, also shows an O signature along the Cu/steel interface associated with the steel, indicating propagation of corrosion along the steel surface at this location. Raman analyses (location 2 in Fig. 16) indicate the oxide formed (possibly

maghemite) is identical to that formed on the steel surface at the base of the defect (location 1 in Fig. 16). It seems likely, but is presently unproven, that the propagation of corrosion along the interface is due to the damaged nature of this location (as shown in Figs. 6 (c), 8 (a), and 9 (a) inflicted during the cold spray coating process. It also should be noted that the cold spray process used to form the coating cannot be considered to be optimized from a manufacturing standpoint.

In on-going studies, the influence of variations in $[O_2]$ on the evolution of the chemistry within a defect is being studied with the long-term goal of determining how damage will accumulate on the steel as repository conditions evolve in the manner depicted in Fig. 3. A particular emphasis is being placed on how damage is distributed along the Cu/steel interface and how this is influenced by the coating process and subsequent coating treatments.

4. SUMMARY

The corrosion of cold spray and electrodeposited coatings has been studied in both anoxic and aerated 3 M NaCl. While minor differences due to the coating morphologies were observed, the corrosion behaviour was similar irrespective of the nature of the Cu.

Under anoxic conditions, the minor amounts of corrosion could be attributed to sulphide, present as an impurity in the salt, which was sequestered as a Cu_2S deposit.

Experiments on a defective coating confirmed that under oxic conditions, O_2 reduction on the surface of the cold spray coating was coupled to corrosion of the exposed steel surface at the base of the defect. The distribution and chemical nature of the corrosion products confirmed that a gradation in solution chemistry existed through the 3 mm-deep defect. The oxidizing conditions maintained active corrosion conditions at the steel surface with the large majority of corrosion product deposits forming on the external Cu surface.

Corrosion was also observed to occur along the Cu-steel interface on coatings produced by the cold spray method. This is most likely due to the damaged nature of the interface produced by the coating process which, presently, has not been optimized.

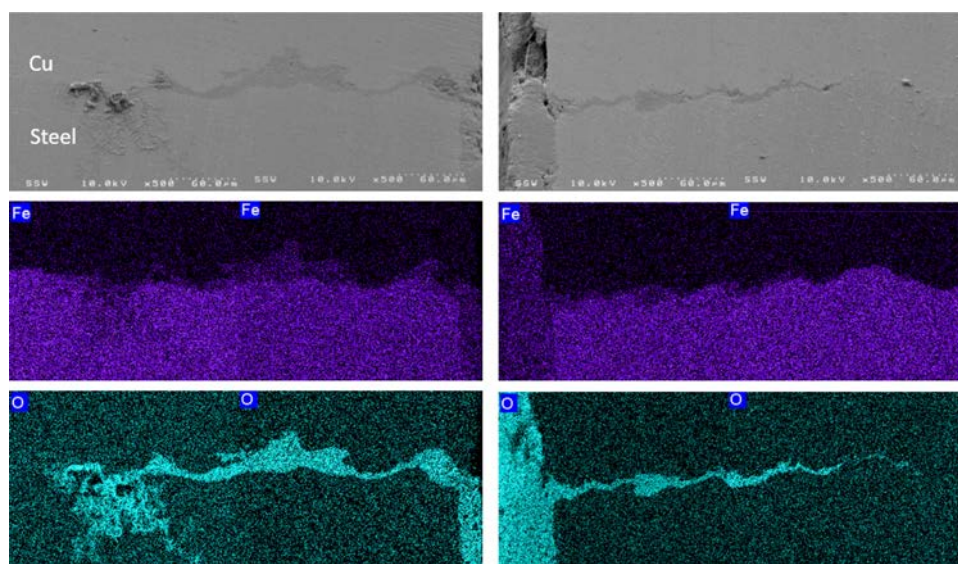


Fig. 19. SEM images and EDX maps recorded at the Cu-steel interface from each side of the coating defect.

ACKNOWLEDGEMENTS

Assistance provided by personnel at Western University's Physics and Engineering Machine Shops, Chemistry Department, and Surface Science Western is gratefully acknowledged. The Nuclear Waste Management Organization (NWMO) provided the funding for this research.

References

- [1] G.M. Kwong, Status of corrosion studies for copper used fuel containers under low salinity conditions, NWMO Technical Report NWMO-TR-2011-14, Toronto, Canada, 2014.
- [2] P.G. Keech, P. Vo, S. Ramamurthy, J. Chen, R. Jacklin, D.W. Shoesmith, Design and development of copper coatings for long term storage of used nuclear fuel, *Corros. Eng. Sci. Technol.* 49 (2014) 425–430, doi:http://dx.doi.org/10.1179/1743278214Y.0000000206.
- [3] P. Jakupi, P.G. Keech, I. Barker, S. Ramamurthy, R.L. Jacklin, D.W. Shoesmith, D.E. Moser, Characterization of commercially cold sprayed copper coatings and determination of the effects of impacting copper powder velocities, *J. Nucl. Mater.* 466 (2015) 1–11, doi:http://dx.doi.org/10.1016/j.jnucmat.2015.07.001.
- [4] R. Partovi-Nia, S. Ramamurthy, D. Zagidulin, J. Chen, R. Jacklin, P. Keech, D.W. Shoesmith, Corrosion of Cold Spray Deposited Copper Coating on Steel Substrates, *Corrosion*. 71 (2015) 1237–1247, doi:http://dx.doi.org/10.5006/1757.
- [5] J. Smith, Z. Qin, F. King, L. Werme, D.W. Shoesmith, Sulfide Film Formation on Copper under Electrochemical and Natural Corrosion Conditions, *Corrosion*. 63 (2007) 135–144, doi:http://dx.doi.org/10.5006/1.3278338.
- [6] J. Chen, Z. Qin, D.W. Shoesmith, Kinetics of Corrosion Film Growth on Copper in Neutral Chloride Solutions Containing Small Concentrations of Sulfide, *J. Electrochem. Soc.* 157 (2010) C338–C345, doi:http://dx.doi.org/10.1149/1.3478570.
- [7] J. Chen, Z. Qin, D.W. Shoesmith, Rate controlling reactions for copper corrosion in anaerobic aqueous sulphide solutions, *Corros. Eng. Sci. Technol.* 46 (2011) 138–141, doi:http://dx.doi.org/10.1179/1743278210Y.0000000007.
- [8] L. Wu, D. Guo, A. Van Belois, J.J. Noël, P.G. Keech, J.C. Wren, Radiation-Assisted Corrosion of Carbon Steel Nuclear Waste Container, *Proc. 17th Int. Conf. Environ. Degrad. Mater. Nucl. Power Syst. –Water React.*, Ottawa, Ontario, 2015.
- [9] P. Vo, D. Poirier, J.-G. Legoux, P.G. Keech, E. Irissou, Application of Copper Coatings onto Used Fuel Canisters for the Canadian Nuclear Industry, in: J. Karthikeyan, C. Kay (Eds.), *High Press. Cold Spray Princ. Appl.*, ASM International, Materials Park, Ohio, USA, 2016.
- [10] P.G. Keech, P. Lin, N. Mahalanobis, Electrodeposited Copper Coatings for Used Fuel Containers, 35th Annu. Conf. Can. Nucl. Soc (2015).
- [11] F. King, C.D. Litke, M.J. Quinn, D.M. Leneveu, The measurement and prediction of the corrosion potential of copper in chloride solutions as a function of oxygen concentration and mass-transfer coefficient, *Corros. Sci.* 37 (1995) 833–851, doi:http://dx.doi.org/10.1016/0010-938X(95)80013-1.
- [12] F. King, C. Lilja, K. Pedersen, P. Pitkanen, M. Vahanen, An update of the state-of-the-art report on the corrosion of copper under expected conditions in a deep geologic repository, *Svens Karnbränlehantering Technical Report SKB TR-10-67* (2010).
- [13] J.M. Smith, J.C. Wren, M. Odziemkowski, D.W. Shoesmith, The Electrochemical Response of Preoxidized Copper in Aqueous Sulfide Solutions, *J. Electrochem. Soc.* 154 (2007) C431–C438, doi:http://dx.doi.org/10.1149/1.2745647.
- [14] J. Chen, Z. Qin, D.W. Shoesmith, Long-term corrosion of copper in a dilute anaerobic sulfide solution, *Electrochim. Acta.* 56 (2011) 7854–7861, doi:http://dx.doi.org/10.1016/j.electacta.2011.04.086.
- [15] C. Cleveland, S. Moghaddam, M.E. Orazem, Nanometer-Scale Corrosion of Copper in De-Aerated Deionized Water, *J. Electrochem. Soc.* 161 (2013) C107–C114, doi:http://dx.doi.org/10.1149/2.030403jes.
- [16] G. Kear, B.D. Barker, F.C. Walsh, Electrochemical corrosion of unalloyed copper in chloride media—a critical review, *Corros. Sci.* 46 (January) (2004) 109–135, doi:http://dx.doi.org/10.1016/S0010-938X(02)00257-3.
- [17] C. Deslouis, B. Tribollet, G. Mengoli, M.M. Musiani, Electrochemical behaviour of copper in neutral aerated chloride solution. I. Steady-state investigation, *J. Appl. Electrochem.* 18 (1988) 374–383, doi:http://dx.doi.org/10.1007/BF01093751.
- [18] V.K. Sharma, F.J. Millero, The oxidation of Cu(I) in electrolyte solutions, *J. Solution Chem.* 17 (1988) 581–599, doi:http://dx.doi.org/10.1007/BF00651464.
- [19] D.L.A. de Faria, S.V. Silva, M.T. de Oliveira, Raman microspectroscopy of some iron oxides and oxyhydroxides, *J. Raman Spectrosc.* 28 (1997) 873–878, doi:http://dx.doi.org/10.1002/(SICI)1097-4555(199711)28:11<873::AID-JRS177>3.0.CO;2-B.
- [20] L. Bellot-Gurlet, D. Neff, S. Réguer, J. Monnier, M. Saheb, P. Dillmann, Raman studies of corrosion layers formed on archaeological irons in various media, *J. Nano Res.* 8 (September) (2009) 147–156, doi:http://dx.doi.org/10.4028/www.scientific.net/jnanor.8.147.
- [21] C.T. Lee, M.S. Odziemkowski, D.W. Shoesmith, An in situ Raman-electrochemical investigation of carbon steel corrosion in Na₂CO₃/NaHCO₃, Na₂SO₄, and NaCl solutions, *J. Electrochem. Soc.* 153 (2006) B33–B41, doi:http://dx.doi.org/10.1149/1.2140680.
- [22] C. Rémaizeilles, P. Refait, On the formation of β-FeOOH (akaganéite) in chloride-containing environments, *Corros. Sci.* 49 (February) (2007) 844–857, doi:http://dx.doi.org/10.1016/j.corsci.2006.06.003.
- [23] M. Bouchard, D.C. Smith, Catalogue of 45 reference Raman spectra of minerals concerning research in art history or archaeology, especially on corroded metals and coloured glass, *Spectrochim Acta – Part A Mol. Biomol. Spectrosc.* 59 (2003) 2247–2266, doi:http://dx.doi.org/10.1016/S1386-1425(03)00069-6.
- [24] A.A. Olowe, J.M.R. Génin, The Influence of concentration on the oxidation of ferrous hydroxide in acidic sulphated aqueous medium: particle size analysis of lepidocrocite, *Corros. Sci.* 32 (1991) 1021–1028, doi:http://dx.doi.org/10.1016/0010-938X(91)90019-L.
- [25] R. Antunes, I. Costa, D. de Faria, Characterization of corrosion products formed on steels in the first months of atmospheric exposure, *Mater. Res.* 6 (2003) 403–408, doi:http://dx.doi.org/10.1590/S1516-14392003000300015.
- [26] X. Liu, F.J. Millero, The solubility of iron hydroxide in sodium chloride solutions, *Geochim. Cosmochim. Acta.* 63 (1999) 3487–3497, doi:http://dx.doi.org/10.1016/S0016-7037(99)00270-7.
- [27] J.C. Hamilton, J.C. Farmer, R.J. Anderson, In Situ Raman Spectroscopy of Anodic Films Formed on Copper and Silver in Sodium Hydroxide Solution, *J. Electrochem. Soc.* 133 (1986) 739, doi:http://dx.doi.org/10.1149/1.2108666.
- [28] T. Kosec, Z. Qin, J. Chen, A. Legat, D.W. Shoesmith, Copper corrosion in bentonite/saline groundwater solution: Effects of solution and bentonite chemistry, *Corros. Sci.* 90 (2015) 248–258, doi:http://dx.doi.org/10.1016/j.corsci.2014.10.017.